Risk Assessment of Cassini Sun Sensor Integrity due to Hypervelocity Impact of Saturn Dust Particles[•]

Allan Y. Lee[1]

Jet Propulsion Laboratory, California Institute of Technology

Pasadena, CA 91109-8099

A sophisticated interplanetary spacecraft, Cassini is one of the heaviest and most sophisticated interplanetary spacecraft humans have ever built and launched. Since achieving orbit at Saturn in 2004, Cassini has collected science data throughout its four-year prime mission (2004–08), and has since been approved for first and second extended missions through September 2017. In late 2016, the Cassini spacecraft will begin a daring set of ballistic orbits that will hop the rings and dive between the upper atmosphere of Saturn and its innermost D-ring twenty-two times. The "dusty" environment of the inner D-ring region the spacecraft must fly through is hazardous because of the possible damage that dust particles, travelling at speeds as high as 31.4 km/s, can do to spacecraft hardware. During hazardous proximal ring-plane crossings, the Cassini mission operation team plans to point the high-gain antenna to the RAM vector in order to protect most of spacecraft instruments from the incoming energetic ring dust particles. However, this particular spacecraft attitude will expose two Sun sensors (that are mounted on the antenna dish) to the incoming dust particles. High-velocity impacts on the Sun sensor cover glass might penetrate the 2.54-mm glass cover of the Sun sensor. Even without penetration damage, craters created by these impacts on the surface of the cover glass will degrade the transmissibility of light through it. Apart from being directly impacted by the dust particles, the Sun sensors are also threatened by some fraction of ricochet ejecta that are produced by dust particle impacts on the large antenna dish (made of graphite fiber epoxy composite material). Finally, the spacecraft attitude control system must cope with disturbances due to both the translational and angular impulses imparted on the large antenna dish and the long magnetometer boom by the incoming high-velocity projectiles. Analyses performed to quantify the risks the Sun sensors must contend with during these hazardous ring-plane crossings are given in this paper.

Acronyms

BLE = *Ballistic Limit Equation*
CDA = *Cosmic Dust Analyzer*
CTH = *Hydrodynamics Simulation Tools (Sandia National Laboratories)*
FP = *Fault Protection*
GFEC = *Graphite Fiber Epoxy Composite*
HGA = *High Gain Antenna*
HITL = *Hypervelocity Impact Technology Laboratory (at JSC)*
HVI = *Hypervelocity Impact*
JSC = *Johnson Space Center*
MEA = *Main Engine Assembly*
MLI = *Multi-layer Insulation*
MMOD = *Micro-meteoroid and Orbital Debris*
RCS = *Reaction Control System*
RPWS = *Radio, Plasma, and Wave Science*
S/C = *Spacecraft*

[•]Copyright 2015 California Institute of Technology. U.S. Government sponsorship acknowledged.
[1]Section Staff, Guidance and Control Section, Division of Autonomous Systems. Mail Stop 230-104, 4800 Oak Grove Drive, Pasadena, CA 91109-8099, USA. Allan.Y.Lee@jpl.nasa.gov.

SEU = *Single Event Upset*
SOI = *Saturn Orbit Insertion*
SSA = *Sun Sensor Assembly*
UV = *Ultra-violet*
XMM = *X-ray Multi-Mirror (an ESA mission)*

Nomenclatures

A_{HGA} = *Total area of the HGA reflector of Cassini (m^2)*
A_{SSA} = *Total area of the two glass covers of the Cassini Sun sensors (m^2)*
C = *Coefficient used in an empirical equation (see Eq. (8))*
D = *Diameter of the (assumed) spherical dust particle (cm)*
D_C = *Diameter of the (assumed) circular crater (cm)*
E = *Kinetic energy of the projectile (Joules)*
E_T = *Compressive strength of the target material (MPa)*
$F(M)$ = *The integral fluence. It is the number of dust particles (per unit area) that impact the spacecraft with mass that equals or is larger than M grams during a specified ring plane crossing*
F_{dark} = *Percent of the crater area that is opaque to Sunline due to fracture-caused total reflection (-)*
F_{ring} = *Number of dust particles impacted on spacecraft (counts per m^2 per crossing)*
f_{SSA} = *Fraction of the ricochet ejecta from HVI impacts of Saturn dust particle on the HGA reflector that affects the Sun sensors (-)*
f_{Mass} = *Ratio of the total mass of the secondary debris relative to mass of incoming particle (-)*
f_{VEL} = *Ratio of the velocity of the secondary debris relative to velocity of incoming particle (-)*
M = *Mass of the dust projectile (gram)*
M_C = *Critical mass of dust particle that will penetrate 50% of the SSA glass cover thickness (gram)*
P_e = *Penetration depth of the HVI on SSA cover glass (cm)*
P_0 = *Theoretical penetration depth of the HVI on glass target as predicted by Eq. (1) (cm)*
V = *Dust particle velocity relative to the S/C (km/s)*
ρ = *Density of the dust particle (gram/cm^3)*
ρ_T = *Density of the target material (gram/cm^3)*
β = *Obliquity angle of the HVI particle on target surface (deg). See Fig. E1 in Appendix E*
Δ = *Momentum transfer multiplication factor (-)*
ν = *Scaling parameter used in Eq. (7) (-)*
μ = *Scaling parameter used in Eq. (7) (-)*
e = *Coefficient of restitution of an elastic collision (-)*

Keywords. Cassini, hypervelocity impact, momentum transfer multiplication factor, optical attenuation due to surface cratering, penetration damage, proximal orbits, Ricochet ejecta, Saturn ring-plane crossing, and Sun sensor.

I. Introduction

Cassini is one of the heaviest and most sophisticated interplanetary spacecraft humans have ever built and launched.[1] Since achieving orbit at Saturn in 2004, Cassini has collected science data throughout its four-year prime mission (2004–08), and has since been approved for a first and second extended missions through September 2017. The orbiter is 6.8 m in height with a "diameter" of 4 meters. The total mass of the spacecraft at launch was approximately 5,574 kg, which included about 3,000 kg of bi-propellant. Fig. 1 depicts the Cassini spacecraft with the deployed magnetometer boom and three RPWS antennas.

In late 2016, the Cassini spacecraft will begin a daring set of ballistic orbits that will hop the rings and dive between the upper atmosphere of Saturn and its innermost D-ring twenty-two times.[2] These orbits are named "proximal" orbits because the spacecraft will be as close as 1,840 km from the 1-bar constant pressure ellipsoidal surface of Saturn. As Cassini plunges past Saturn, the spacecraft will collect rich and valuable data that will better our understanding of Saturn's gravity and magnetic fields, and atmospheric sciences. No other missions has explored this unique region so close to the planet. Details of the proximal orbit design are given in Refs. 2–3. With help from the public, members of NASA's Cassini mission to Saturn have chosen to call the spacecraft's final orbits the *Grand Finale*.

Key engineering challenges that must be overcome to achieve a successful *Grand Finale* are summarized in Ref. 3. These challenges are all related to the "not-well-understood" environment between the inner D-ring and the upper atmosphere of Saturn. The "dusty" environment that the spacecraft must fly through is hazardous because of the damage dust particles, travelling at speeds as high as 31.4 km/s, can do to spacecraft hardware. The adequacy of the control authority of the spacecraft attitude control thrusters (or reaction wheels) relative to the atmospheric torque that will be imparted on the spacecraft during low-altitude flybys must also be carefully addressed. The atmospheric torque is related to the squared S/C velocity relative to Saturn (which is as high as 31.4 km/s) as well as the "not-well-characterized" atmospheric density. Finally, the radiation environment of the inner D-ring must also be considered. High-energy ion/proton that are trapped in this environment have the potential to trigger single event upsets (SEU) of various attitude control sensors and actuators on the spacecraft. Vulnerable equipment includes the inertial reference units (gyro's), stellar reference units (star trackers), Sun sensors, reaction wheels, and their associated solid-state power switches. Hence, thresholds and persistence limits of various fault protection (FP) error monitors must be selected to be robust to these transient SEU events. In this paper, we focus on assessing the potential performance degradation of the Cassini Sun sensor due to hypervelocity impact (HVI) of the D-ring dust particles.

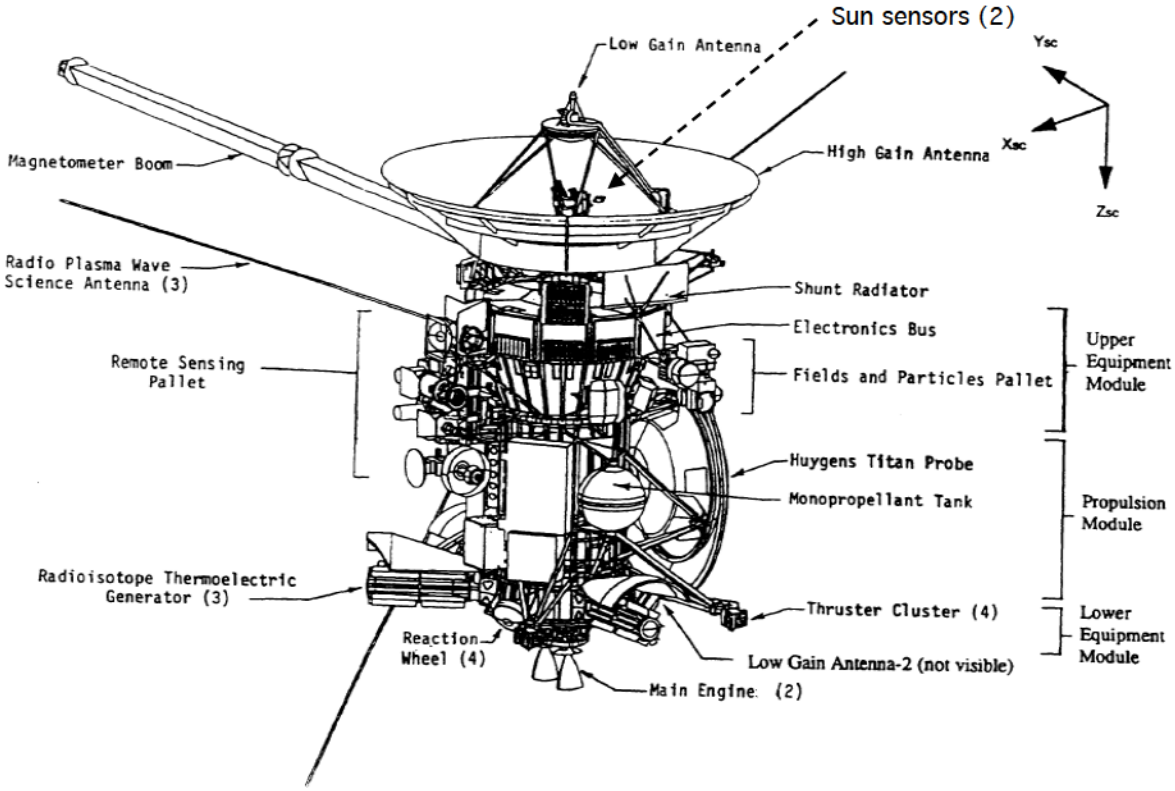

Fig. 1. Cassini Spacecraft Cruise Configuration[1]
(MLI and main engine cover have been removed from the image for clarity)

II. Dust Hazard Management During Cassini Ring Plane Crossings

All of the outer planets have ring systems, and most of them are believed to contain some dust particles that are large enough to pose a hazard to spacecraft via hypervelocity impacts on science or engineering instruments. The rings of Saturn are dense and complex[3,4] and the proximal orbital flybys must be designed taken into consideration the risk posed by the ring dust particles.

Two sources of knowledge are needed to estimate the risk of dust HVI on spacecraft. The ring dust particle environment through which the spacecraft must fly through must be quantified. This will involve predicting the dust particle integral fluence (cumulative number of dust particles with a given mass or larger, per unit exposed area and

time) using a ring model. The ring model incorporates all scientists' understanding of the abundance and size of materials of the Saturnian rings. Both Earth-based and spacecraft-based measurements are incorporated in this model.[4] Risk assessment of dust HVI also requires a detailed knowledge of the spacecraft layout. That is, the vulnerability of all external surfaces to dust impacts, the locations of all critical hardware with respect to these external surfaces, and the mechanism by which impacting material may reach this hardware.

As depicted in Fig. 2, most surfaces of Cassini are covered by MLI (multi-layer insulation). When a dust particle strikes the MLI, even a surface that may seem superficially flimsy, it vaporizes into a shower of many smaller particles.[5] For setback distances more than a few centimeters, even thermal blanketing provides substantial protection of any surface it shields. Toughening materials, such as ceramic fabric and high-strength fabric, have been included within the MLI thermal blanket that is commonly used to provide passive thermal control of spacecraft hardware. These additional materials provide improved micrometeoroid shielding. Since MLI covers the bulk of the spacecraft (see Fig. 2), the single set of surfaces that alone drives the spacecraft vulnerability is areas on the electronics bus that are not covered by MLI. These areas must be protected by other means.

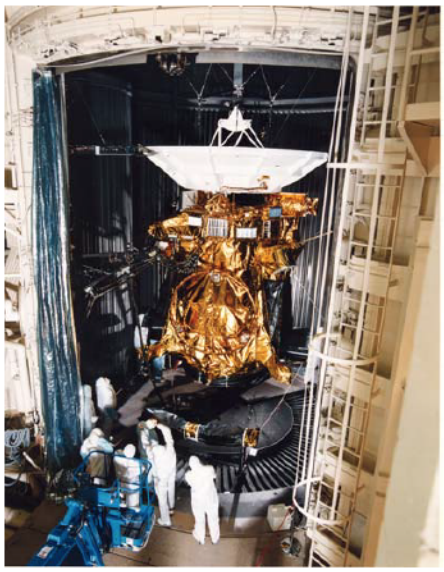

Fig. 2. Cassini Solar Thermal Vacuum Test Configuration (The magnetometer boom and Huygens Probe have been removed)[7]

The other critical spacecraft components that are most vulnerable to dust impacts are the redundant main engine nozzles. Particle impacts can spall, pit, or penetrate the sensitive disilicide columbium coating that the engines require for proper engine thrusting burn. With Cassini now in a stable Saturn orbit, loss of the main engines alone does not cause end of mission, but it will severely limit the orbit geometries available to the mission and some scientific objectives will not be met. The main engines were critical to achieving Saturn orbit, and prior to launch Cassini was equipped with a single main engine assembly (MEA) cover to protect against micrometeoroid impacts.[6] The MEA cover was closed during most of the cruise to Saturn, and is also closed during hazardous ring plane crossings at Saturn. Hazardous crossings are those where the estimated dust particle risk is significant. Special care is taken to ensure the MEA cover is adequately stowed (open) prior to a main engine ΔV burn. At Saturn, the cover is normally kept open until the next hazardous crossing. To be conservative, for all proximal ring plane crossings, the MEA cover will be deployed (i.e., covered the engines). This will allow the spacecraft to fly science-friendly attitudes while still protecting the engines.

Unlike the engines, the high gain antenna (HGA) is relatively insensitive to impacts of millimeter-sized (or smaller) dust particles. Even the antenna feeds can tolerate a peppering of millimeter-sized holes with almost no loss in transmission capability.[4] The wavelengths Cassini uses for communication (X-band), RADAR science (Ku-band), and Radio science (Ka-band) are long enough that millimeter-sized holes in feeds or reflective surfaces cause almost no appreciable degradation. The HGA therefore constitutes a protective surface for Cassini. As such, the HGA-to-RAM pointing strategy was selected by the mission operations team for the two ring plane crossings performed before/after the Saturn Orbit Insertion (SOI) burn in 2004 (as well as several other ring plane crossings listed in

Table 1).[1] Here, the term "RAM" referred to the S/C's velocity vector relative to the ring particles. Moreover, the bore-sight vectors of both the Cassini's star trackers and the science cameras are mounted perpendicular to the HGA axis.[1] Hence, the HGA-to-RAM pointing strategy will minimize the probability of micrometeoroid damage to both the trackers and science cameras.[a] In summary, two key factors to consider for a safe ring plane crossing are: [1] the location of the ring plane crossing and [2] the spacecraft attitude at the time of the ring plane crossing. The former determines the integral fluence of the dust particles, and the later determines the exposure of vulnerable spacecraft components to HVI.

Table 1 Ring Plane Crossings With HGA-to-RAM S/C Attitude and MEA Cover Deployed

Critical Ring Plane Crossings	
Ring Regions*	Date
G	7/1/04
JE	7/1/04
JE	7/1/04
G	7/1/04
E	3/9/05
G	4/14/05
E	9/23/05
G	6/11/07
G	6/28/07
JE	6/28/07
G	1/27/10
G	2/13/10
G	6/19/10
JE	11/24/15
JE	12/6/15
JE	12/11/16
JE	1/2/17
D	4/26/17
D	5/28/17
D	6/4/17
D	6/29/17
D	7/6/17

*Locations of the D, E, F, G, and JE rings are depicted in Fig. 3.

III. Hypervelocity Impacts of Dust Particles on Glass Covers of Cassini Sun Sensors (near SOI)

The proximal orbits will not be the first time the Cassini spacecraft must contend with this hazard potential. After an interplanetary cruise that lasted 6.7 years, the Cassini spacecraft arrived at Saturn on June 30, 2004. Cassini approached Saturn from below the ring plane and crossed through a gap between the F and G rings of Saturn. This so-called Ascending Ring-Plane Crossing occurred about 25 minutes before Cassini began firing its main rocket engine to slow its velocity sufficiently to be captured by the gravity field of Saturn. Following this Saturn Orbit Insertion (SOI) burn, Cassini imaged Saturn and the rings and then prepared for the Descending Ring-Plane Crossing which occurred 105 minutes after the end of the SOI burn.[1,3] During these hazardous Saturn ring-plane crossings, the high-gain antenna (see Fig. 1) is pointed parallel to the velocity vector of the orbiter (relative to the ring particles) in order to protect most of spacecraft instruments from the incoming energetic ring particles. This proven strategy has subsequently been adopted for all G ring crossings and for five of the twenty-two proximal orbital D-ring flybys in 2017 (see Table 1) and contingency commands are in place for the other 17 crossings if needed (see also Section VII). Unfortunately, this attitude will "expose" the two Sun Sensor Assemblies (SSA, that are mounted on the high-gain antenna, see Fig. 1) to incoming dust particles. Risk to Sun sensor assemblies during

[a]Ref. 9 provided an overview of micrometeoroid damage to the optical detectors on the XMM-Newton and Swift spacecraft.

HGA-to-RAM F/G-ring (SOI) is addressed in this section. That of the D-ring (proximal orbit) crossings will be addressed in Section IV. Momentum transfer from incoming high-velocity dust particles onto the spacecraft's HGA dish and magnetometer boom will be addressed in Section V. Direct impacts of dust particles on the glass Sun sensor covers are a threat, as well as secondary impacts of debris scattered off other High Gain Antenna surfaces. That risk will be addressed in Section VI.

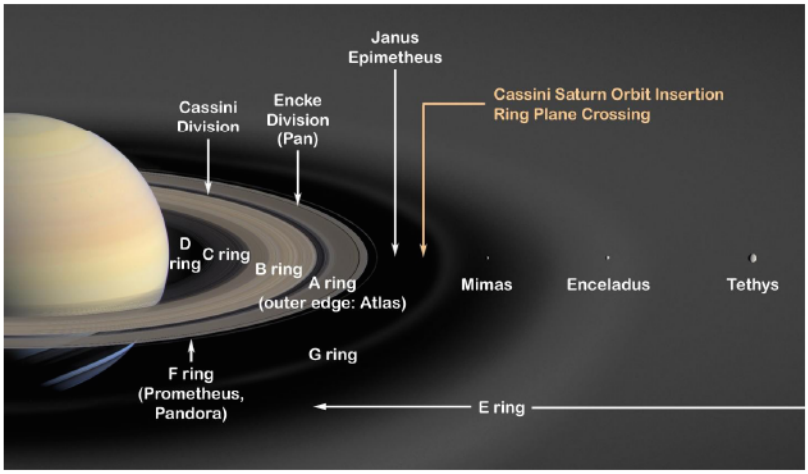

Fig. 3. The Rings of Saturn (from Ref. 3)

In the HGA-to-RAM attitude, the magnetometer boom (see Fig. 1) will also be exposed to incoming dust particles. But the 10-m magnetometer boom mast is covered with black Kapton, and both the inboard and outboard magnetometers are shielded from Sunline and dust particles by aluminized Kapton shades. The Cassini radio and plasma wave (RPWS) investigation is designed to study radio emissions, plasma waves, thermal plasma, and dust in the vicinity of Saturn. The three monopole electric field antennas are conducting cylinders, each 10 m long and 2.86 cm in diameter.[8] The antennas are made of beryllium-copper, silver plated on the exterior surface, and painted black on the interior for thermal control. Approximately 12% of the surface area is perforated with small holes for better thermal control. In the HGA-to-RAM orientation, only two of the three antennas are exposed to the incoming dust particles because the third antenna will be in the "shadow" of the magnetometer boom. Designed to investigate dust in the vicinity of Saturn, the RPWS antennas are immune to HVI.

The Cassini SSA's are placed inside two aluminum housings that are located on the HGA (see Fig. 1). A glass window protective cover (with thickness of 2.54 mm or 0.1 inches) is used for each SSA to seal the sensor from the external environment (but to allow Sunlight to get to the SSA). These windows are made of radiation-resistant glass. They can absorb solar UV rays and thus eliminate the possibility of UV damage within the sensor heads. There are two types of SSA risks during ring plane crossings. The first risk is related to penetration failure of the SSA cover glass due to impacts by Saturn ring dust particles. The second risk is related to the degradation in the SSA performance (optical attenuation) due to impact craters created by HVI. Image of an impact crater due to a 1-mm diameter aluminum projectile travelling at 5.11 km/s on a 2.5-cm thick soda lime glass blank is depicted in Fig. 4 (Ref. 10). Relative to metallic target surfaces, a HVI on a glass target is far more dramatic. This is because the shock pressure produced by HVI is significantly larger than the low tensile strength of glass. Tensile stresses released on reflections from the free surfaces will dominate the material strength over distances several times the diameter of the high-speed projectiles.

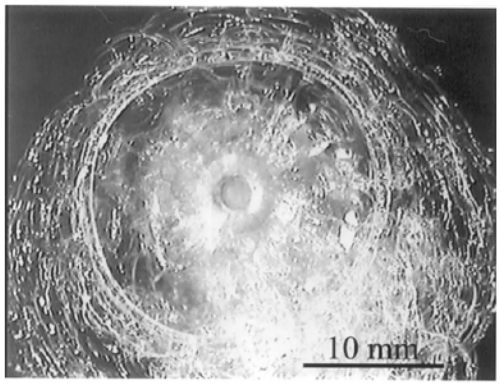

Fig. 4. Damage due to Solid Particle Hypervelocity Impact on Glass Surfaces (from Ref. 10)

Penetration depth in glass due to micro-particle impact is related to both the density and diameter of the projectile, and the relative impact velocity. From Ref. 10–11, the basic equation that is used for predicting penetration depth is given by Eq. (1).

$$P_0 = 0.53\, D^{1.06} \rho^{0.5} V^{0.6667} \qquad (1)$$

Here, P_0 is the theoretical penetration depth measured from the top surface in cm, D is the projectile diameter in cm, ρ is the projectile density in g/cm^3, and V is the projectile velocity in km/sec. See Fig. 5 for a graphical illustration of these variables.

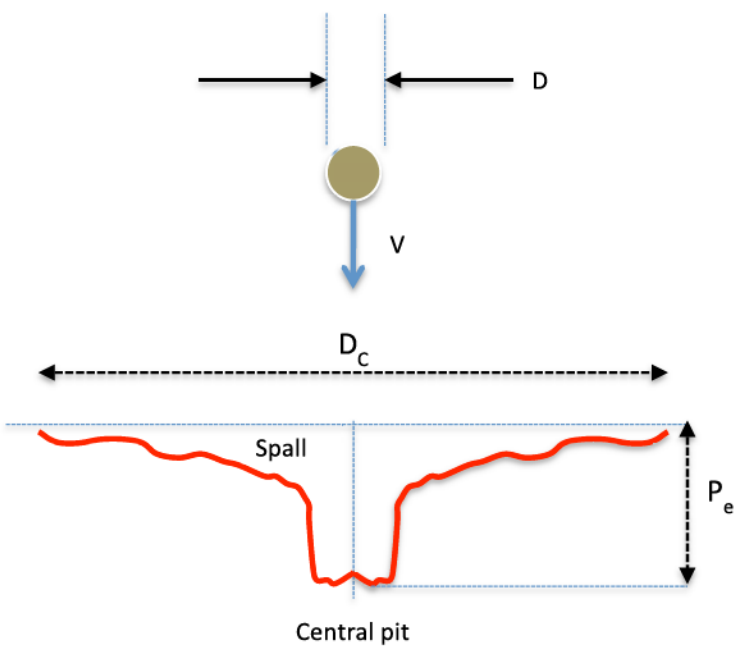

Fig. 5. Side View of an HVI-generated Crater and its Dimensions
(D is the diameter of the projectile, V is the velocity of the projectile, P_e is the penetration depth of the HVI crater, and D_c is the diameter of the spalled surface crater)

For hypervelocity impacts (with 6.0≤V≤7.5 km/s), experimental calibration of Eq. (1) led to a correction factor of 1.99 in Eq. (2).[11]

$$P_e = 1.99 \times 0.53\, D^{1.06} \rho^{0.5} V^{0.6667} = 1.0547 \left[\frac{6M}{\pi\rho}\right]^{0.3533} \rho^{0.5} V^{0.6667} \quad (2)$$

Note that in the revised expression, the projectile diameter is replaced by a term that is related to the mass and density of the projectile ($D = [6M/\pi\rho]^{1/3}$). This is done because the ring dust integral fluence (particles per area per

crossing), to be addressed in the following, is a function of the dust mass. The uncertainty associated with the experimental factor is 1.99±0.07.

For the F/G ring plane crossings at SOI, the mean relative velocity is estimated to be 17.1 km/s. The mean density of the dust particles was estimated to be 0.5 gram/cc.[12] This estimate is lower than the density of water, which is the major constituent of the Saturnian rings. Possible explanation for this density estimate is that the dust particles are porous. But to be conservative, all computations will be made with higher density estimates of 1.0 and 2.0 gram/cm^3. Using Eq. (2), we note that only dust particles with masses that are larger than 8.1e-6 gram will generate craters with depths that are larger than 1.27 mm. This is half the thickness of the window glass of the SSA. It is assumed that only penetration depth that is larger than this thickness threshold will lead to Sun sensor damage.[13–14] Else, the window glass of the SSA has protected the SSA against the HVI. If the assumed dust density is 1.0 and 2.0 gram/cc, the threshold mass of the dust particles (that will penetrate 50% of the cover glass) are 6.16e-6 and 4.70e-6 gram, respectively.

Two assumptions were made in doing these calculations. It is assumed that Eq. (2), which has been validated against HVI test results with impact velocity of 6.0–7.5 km/s, is equally applicable to HVI as high as 17.1 km/s at SOI. This assumption is made based on the reasoning given in Appendix A. It was further assumed that the HVI was normal to the glass covers. In Ref. 16, the dependency of HVI impact depth with the obliquity angle (angle between the velocity vector and the surface normal) was given. In that paper, data are reported for hypervelocity impact cratering in glass arising from impacts of 1 mm diameter aluminum spheres impacting thick glass targets at 5.11±0.13 km/s. The obliquity angle of the projectiles was varied from 0° (normal incidence) to 80° (glancing incidence). For obliquity angle of 60°, the crater depth is about 81% of that measured with normal HVI.[16] Based on results reported in Ref. 16 (see also Ref. 13, etc.), one can conclude that penetration depth predicted using Eq. (2) that is used in this study represents the worst case.

The integral fluence of Saturn dust particles for all the ring plane crossings in the prime mission, as a function of dust particle mass, is depicted in Fig. 6 (see Ref. 12). Best pre-launch knowledge of Saturn ring dust particle environment is captured in Ref. 12, which is the Cassini environment design requirement document.[v] In this size distribution figure (Fig. 6), the ordinate gives the number of dust particles (per unit area) that impact the spacecraft with masses that equal or are larger than the mass given by the abscissa. In Fig. 6, the blue dots give the integral fluence for all ring plane crossings in the prime mission. It could be approximated by the expression $F(M) = 1.7366e\text{-}5 \times M^{-0.973}$.[a] For example, the number of dust particles with masses that are larger than 1.0e-9 gram is 9,924 counts per squared meter. In the same figure, the red dots give the integral fluence for the two SOI ring plane crossings. It could be approximated by the expression $F(M) = 1.479827e\text{-}5 \times M^{-0.833}$. For example, the number of dust particles with masses that are larger than 1.0e-9 gram is 468 counts per squared meter. Obviously the integral fluence for all crossings during the mission is greater than that for just the two SOI ring plane crossings. To be conservative, we will use the integral fluence (for all crossings) in most of the following computations. The integral fluence for the D-ring crossings, also given in Fig. 6, is higher than its F/G-ring counterpart. The integral fluence for the D-ring crossings will be used in Section IV to assess the risk of the Sun sensors due to HVI impacts.

[v]For post-launch knowledge of the integral fluence of Saturn dust particle, please refer to Ref. 33 and the references cited therein.

[a]This is a straight-line approximation (in log-log scale) that bounds the integral fluence given in Ref. 12.

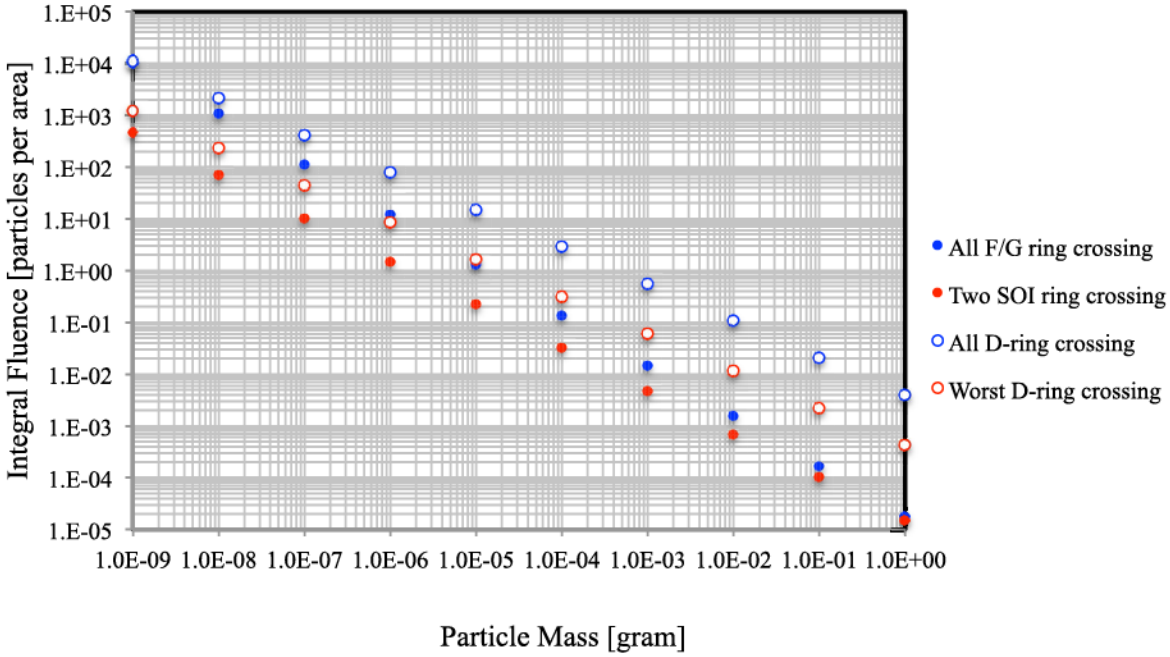

Fig. 6. Saturn dust integral fluence (particles per unit area) as a function of particle mass (F/G and D-ring plane crossings)[12]

From Fig. 6, the integral fluence for particles with mass sizes that are greater than 8.1e-6 gram (particles with this mass will generate craters with penetration depth of ≥1.27 mm) is less than 1.56 particles/m^2. Since the glass cover area of the two Sun sensors (A_{SSA}) is 4.6e-4 m^2, the number of dust particles that could penetrate 50% of the thickness of the glass cover is 1.56×4.6e-4 or 7.18e-4 particles. This probability is practically zero. If the density of the dust particles is quadrupled from 0.5 to 2.0 gram/cc, the corresponding number of dust particles with masses that could penetrate 50% of the thickness of the glass cover is 1.22e-3 particles. Again, this probability is practically zero. In Ref. 12, there are two safety-related requirements that are applicable to the ring plane crossing scenarios. The requirement on penetration damage due to solid particles stated that: "*The flight system shall be designed to ensure a 95% probability of mission success in the solid particle environment specified in Fig. 6.*" Since the computed number of dust particles that will damage the cover glass is <<1 particle, it is our assessment that the above stated penetration damage requirement is met.

Craters created by HVI on the surface of the SSA cover glass will degrade the transmissibility of light through it. Experimental results[11] indicated that less than 10% (f_{dark}) of the damage area has fractures that caused total light reflection. Also, the SSA vendor estimated that only craters with diameters that are >0.762 mm will affect SSA output. To estimate the dust particle mass that will produce craters with 0.762-mm diameter (D_c), we used the following expression (again, from Ref. 11):

$$D_c = 8.037\left[\frac{6M}{\pi\rho}\right]^{0.3533}\rho^{0.5}V^{0.6667} \quad (3)$$

Here, D_c is the estimated crater diameter in cm. With reference to Eq. (2), we note that D_c = 7.62 P_e (penetration depth) which is a key conclusion of Ref. 11. For all the ring plane crossings of the Cassini prime mission, the mean relative velocity (V) is estimated to be 13.6 km/s. The mean density (ρ) of the dust particles was estimated to be 0.5 gram/cc. Using Eq. (3), the dust mass that will generate crater diameter of 0.762 mm is 0.955e-8 gram. For a density of 2.0 gram/cc, the critical mass becomes 0.535e-8 gram.

The total crater area, as a function of the SSA cover glass area, is estimated in Eq. (4).

$$\text{Attenuation} = \frac{2}{A_{SSA}} \int_{M_C=0.955\times10^{-8}}^{M=10^{0}} f_{dark}[-\frac{\partial F_{ring}(M)}{\partial M} A_{SSA}] \frac{\pi}{4} D_c^2(M)\, dM \tag{4}$$

$$= 0.037\%$$

$$= 0.064\% \quad (\text{if } \rho \text{ is quadrupled, } M_C \text{ is 0.535e-8 gram})$$

In Eq. (4), the crater diameter (D_c), in units of cm, must be converted into meters in computing the optical attenuation factor. The term $\partial F/\partial M$ (which is a function of the dust particle mass) is used to compute the number of dust particles that impacted the SSA cover glass. Also, note the use of a factor of 2 to be conservative. The computed attenuation factor is 0.037–0.064%, which is small. Details of these calculations are given in the Appendix B. Note in Appendix B the term $\partial F/\partial M$ was computed using the integral fluence for all ring plane crossings (worst case). In Ref. 12, beside the penetration damage requirement stated above, there is another surface damage requirement that is also applicable to the ring plane crossing scenarios. It stated that: "*For an assembly with exposed optics or with critical thermal surface where the product of integral fluence (from Fig. 6) and sensitive exposed surface area is significantly larger than 1, the assembly shall be designed to ensure an acceptable level of surface property degradation when exposed to twice the fluence given in Fig. 6.*" Since the computed optical attenuation factor is <<0.1% (even with a factor margin of 2 in Eq. (4)), it is our assessment that the above stated surface damage requirement is also met.

Beside Ref. 11, other empirical relations between the crater diameter (D_c, in cm) and the density of the projectile (ρ, in gram/cc), the mass of the projectile (M, in gram), and the relative velocity (V, in km/s) are also available in the literature. See, in particular, Refs. 13, 17–21. A side-by-side comparison between these empirical relations is given in Eq. (5).

$$D_c = 8.037[\frac{6M}{\pi\rho}]^{0.3533}\rho^{0.5}V^{0.6667} \qquad \text{Flaherty (Ref.11), 1970}$$

$$D_c = 30.9[\frac{6M}{\pi\rho}]^{0.443}\rho^{0.44}V^{0.44} \qquad \text{Edelstein (Ref. 17), 1995}$$

$$D_c = 9.656[\frac{6M}{\pi\rho}]^{0.394}\rho^{0.373}V^{0.915} \qquad \text{Burt and Christiansen (Ref. 18), 2003}$$

$$D_c = 5.3[\frac{6M}{\pi\rho}]^{0.3533}\rho^{0.5}V^{0.6667} \qquad \text{Christiansen (Ref. 13), 2009} \tag{5}$$

$$D_c = 2.16[\frac{6M}{\pi\rho}]^{0.359}\rho^{0.784}V^{0.727} \qquad \text{Paul, Igensbergs, and Berthoud (Ref. 19), 1997}$$

$$D_c = 8.49[\frac{6M}{\pi\rho}]^{0.4}\rho^{0.42}V^{0.29} \qquad \text{Taylor and McDonnell (Ref. 21), 1997}$$

In Eq. (5), Burt and Christiansen performed HVI tests on high-purity fused silica monoliths used in the space shuttle windows using 0.4-mm diameter Al 2017-T4 projectiles at 2.5–7 km/s.[18] Accordingly to Ref. 20, results from Ref. 18 are found to provide the most conservative prediction of the crater diameter. The NASA Johnson Space Center (JSC) Ballistic Limit Equation (BLE) for HVI induced crater depth and diameter[13] is also listed in Eq. (5) (see the expression under Christiansen 2009). The spall diameter predicted by Refs. 19 and 21 are small relative to those predicted by other references. For the SOI ring plane crossings, with estimated dust particle density ρ of 0.5 gram/cc and V = 13.6 km/s, a graphical comparison of these relations is given in Fig. 7. For particle mass within the range of 1.0e-9<M<1.0e-3 gram, crater diameter predicted by Ref. 18 (Burt and Christiansen, 2003) produced the most conservative result. Crater diameter predicted by Eq. (3) (Ref. 11, 1970) produced the second most conservative result for particle range of 1.0e-9<M<2.0e-5 gram. Optical attenuation error computed according to the most conservative results given by Ref. 18 is given in Appendix C. The computed attenuation error, 0.083–0.089%, is larger than that produced using Eq. (3), which is 0.037–0.064% (Appendix B). However, both ranges of attenuation error are very small and they do not threaten the SSA performance.

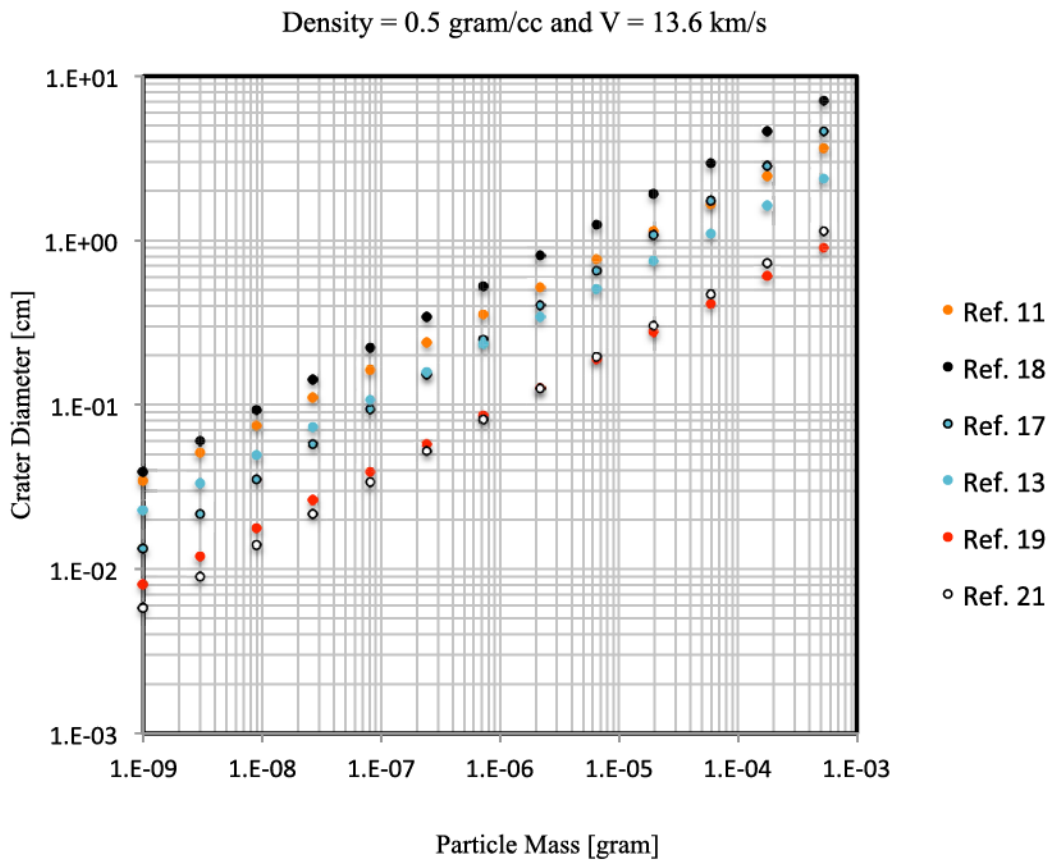

Fig. 7. Variation of crater diameter with impact particle mass based on six different HVI models

IV. Hypervelocity Impacts of Dust Particles on Glass Covers of Cassini Sun Sensors (Proximal Orbits)

In late 2016, the Cassini spacecraft will begin a daring set of ballistic orbits that will hop the rings and dive between the upper atmosphere of Saturn and its innermost D-ring twenty-two times.[2,3] These orbits are named "proximal" orbits because the spacecraft will be as close as 1,840 km from the 1-bar constant pressure ellipsoidal surface of Saturn. As Cassini plunges past Saturn, the spacecraft will collect rich and valuable data that will better our understanding of Saturn's gravity and magnetic fields, and the planet's upper atmosphere. No other missions has explored this unique region so close to the planet.

The proximal orbits will span from April 23 to September 15, 2017. In five of the 22 orbits, the spacecraft will fly very close to the innermost D-ring (with distance from the Saturn center of 64,000 km). The five orbits are orbit 1, 6–7, and 11–12 (see also Table 1). For these orbits, the Cassini mission operations will again employ the HGA-to-RAM pointing strategy. Hence, an assessment of the risk of the Cassini SSA due to hypervelocity impact by the ring dust particles must again be made. David Seal, the cognizant engineer for dust hazards on the Cassini project, has supported this study with his estimation of the integral fluence of the D-ring crossings. Following his recommendations, we use the following parameters in this study: Impact velocity is bounded by 31.4 km/s and the dust particle density is bounded by 1 gram/cm^3 (for the SOI ring plane crossings, the density assumed a range of 0.5–2 gram/cm^3. See Section III). The integral fluence of ring dust particles for all D-ring crossings are given in Fig. 6 (the blue and red "hollow circles"). The blue hollow circle's denote the integrated fluence of all D-ring crossings and it could be approximated by $F(M)=3.9703267e\text{-}3\times M^{-0.71486}$ particles per unit area. The red hollow circle's denote the integrated fluence of the worst D-ring crossing and it could be approximated by $F(M)=4.191642e\text{-}4\times M^{-0.71670}$ particles per unit area. Relative to the integral fluence for all F/G ring plane crossings, the D-ring fluence is larger for all particle mass that is >1.0e-9 gram. At a particle mass of 1.0e-5 gram, the D-ring fluence (for all crossings) is a factor of 11.7 higher than that of F/G-ring fluence (for all crossings).

For hypervelocity impacts (with $6.0\leq V\leq 7.5$ km/s) on glass, experimental results led to the penetration depth

equation of Eq. (2).[11] For the D-ring plane crossings of proximal orbits, the mean relative velocity is estimated to be 31.4 km/s. Using Eq. (2), and assuming a dust density of 1 gram/cm^3, we determine that only dust particles with masses that are larger than 1.97e-6 gram will generate craters with depths that are larger than 1.27 mm (this is half the thickness of the window glass of the SSA). It is assumed that only penetration depth that is larger than this threshold will lead to Sun sensor damage.[13–14]

From Fig. 6, the integral fluence (all D-ring crossings) for particles with masses that are greater than 1.97e-6 gram is less than 47.586 particles/m^2. Since the glass cover area for both SSA (A_{SSA}) is about 4.6e-4 m^2, the number of dust particles that could penetrate 50% of the thickness of the glass cover is 47.586×4.6e-4 or 0.0219 particles. Again, since the computed number of dust particles that will damage the cover glass is <<1 particle, it is our assessment that the penetration damage requirement stated in Section III will also be met during the D-ring crossings. However, the penetration damage probability during the D-ring crossing is two orders of magnitude larger than that of SOI F/G-ring crossings.

Using Eq. (3), and assuming a mean relative velocity of 31.4 km/s and a mean dust particle density of 1.0 gram/cc, the dust mass that will generate crater diameter of 0.762 mm is 1.49e-9 gram. The total crater area, as a function of the SSA cover glass area, is estimated using an expression similar to Eq. (4). Based on the detailed calculations given in Appendix D, and for integral fluence of all the D-ring crossings, the computed optical attenuation factor is 0.998%. The integral fluence for a single (but worst) D-ring crossing is given in Fig. 6 (see the white dots). For that worst-case D-ring crossing, the computed optical attenuation factor is 0.1076%. A summary of all results is given in Table 2. Based on results given in this table, we judge that all HVI-related mission risk requirements of Cassini are met.

Table 2 Summary of All Ring Plane Crossing HVI Risk

F/G Ring Crossings	
Number of particles that can damage SSA cover glass in all F/G ring plane crossings (density is 0.5–2 gram/cc).	7.18e-4 – 1.22e-3 particles
Fraction of SSA cover glass area blacked-out by HVI craters due to total reflection using results from Ref. 11 (density is 0.5–2 gram/cc).	0.037 – 0.064%*
Fraction of SSA cover glass area blacked-out by HVI craters due to total reflection as computed using results from Ref. 18 (density is 0.5–2 gram/cc).	0.083 – 0.089%*
D Ring Crossings	
Number of particles that can damage SSA cover glass in all D ring plane crossings (density is 1 gram/cc).	2.19e-2 particles
Fraction of SSA cover glass area blacked-out by HVI craters due to total reflection (all D-ring plane crossings with density of 1 gram/cc) using results from Ref. 11.	0.998%*
Fraction of SSA cover glass area blacked-out by HVI craters due to total reflection (A single worst-case D-ring crossing with density of 1 gram/cc) using results from Ref. 11.	0.1076%*
Fraction of SSA cover glass area blacked-out by HVI craters due to total reflection (A single worst-case D-ring crossing with density of 1 gram/cc) using results from Ref. 18.	0.4371%*

*Computed with a factor of 2 margin.

V. Momentum Transfer in Hypervelocity Impacts

During a ring plane crossing, the spacecraft will encounter dust particles that impart impulsive forces on the spacecraft. In the HGA-to-RAM ring-plane crossing attitude, the two key spacecraft surfaces that will experience these collisions are the parabolic HGA dish and the magnetometer boom. The projected areas of the HGA and the "exposed" magnetometer are 12.57 and 4.32 m^2, respectively.[#] The small projected areas of the three RPWS antennas (<1 m^2, total) have been neglected in this study. For the purpose of force and momentum calculations, it is

[#]Some portion of the 10-m magnetometer boom will be "shielded" by the HGA dish in the HGA-to-RAM attitude.

necessary to estimate the mass flux rate of dust particles imparted on these surfaces. In this study, we will focus on the mass flux rate for the worse case D-ring crossing (see Fig. 6).

From Sections III and IV, the integral fluence F(M) is defined as the number of dust particles with mass ≥M that impacted on spacecraft (particle counts per unit area per crossing). Hence, the number of dust particles with mass M, per unit area and crossing is given by $-\partial F/\partial M$. For the worst-case D-ring crossing, the mass flux rate is given by Eq. (6).

$$
\begin{aligned}
&F = e^{a_0} M^{a_1}, \qquad a_0 = -7.7772479,\ a_1 = -0.7167029 \\
&\frac{\partial F}{\partial M} = a_1 e^{a_0} M^{a_1 - 1} \\
&\frac{dM}{dt} = \text{Total mass of dust particles imparted on S/C for the worst D-ring crossing} \\
&= \int_{M_1}^{M_2} M\{-\frac{\partial F}{\partial M}\} A_{project}\ dm = \int_{M_1}^{M_2} M\{-a_1 e^{a_0} M^{a_1 - 1}\} A_{project}\ dm = \{\frac{a_1}{1+a_1}\} e^{a_0} A_{project} (M_1^{a_1+1} - M_2^{a_1+1}) \\
&\text{where } A_{project} \text{ is the projected area of either the HGA or the magnetometer boom}
\end{aligned}
\tag{6}
$$

With $M_1 = 10^{-9}$ gram and $M_2 = 1$ gram (see Fig. 6), the mass flux rates experienced by the HGA and the magnetometer boom are 1.329e-2 and 4.568e-3 gram per crossing, respectively.[v]

Hypervelocity impacts onto solid materials like Graphite Fiber Epoxy Composite (GFEC) material of the Cassini HGA dish are characterized by significant amount of debris ejected backward. This process causes an effect called "momentum transfer multiplication" to occur. That is, the momentum change of the target is larger than the momentum of the incoming projectile. A schematic representation of the secondary debris for normal, oblique, and grazing HVI are depicted in Fig. 8.

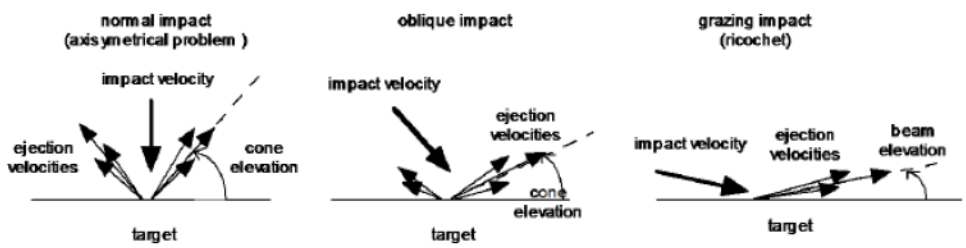

Fig. 8 Schematic representation of debris cone for normal, oblique, and grazing HVI (from Ref. 23)

The efficiency of the momentum transfer is expressed in term of a momentum multiplication factor (Δ, unit-less). It is defined as the ratio of the change in target momentum relative to the momentum of the incoming projectile. For *purely elastic* impacts, the momentum transfer efficiency Δ is only related to the coefficient of restitution *e*: Δ =1+e. If e = 0.8, Δ=1.8. That is, the momentum imparted on the target is about 80% larger than that of the incoming projectile. For non-elastic HVI, the dependency of Δ on the projectile velocity and projectile/target material properties must be estimated via experimental data. Ref. 24 provided the following relation:

$$\Delta - 1 = K\{\frac{\rho_T}{\rho}\}^{1-3\nu}\{V\sqrt{\frac{\rho_T}{E_T}}\}^{3\mu-1} \tag{7}$$

In this equation, ρ_T and ρ (in gram/cc) are the densities of the target and projectile materials, respectively. E_T (in MPa, mega-Pascal) is the compressive strength of the target material, and K, ν, and μ are unit-less scaling parameters. For the GFEC material of the Cassini HGA dish, ρ_T =1.8 gram/cc and E_T =306 MPa.[25] For the worse case D-ring crossing, ρ =1.0 gram/cc, and V =31.4 km/s. Approximate magnitudes of scaling parameters for GFEC materials are: K = 0.047, ν = 0.4, and μ = 0.61.[24] Back substitutions of these values into Eq. (7) lead to a momentum

[v]If the upper bound of the dust mass is ten times larger, M_2 = 10 gram, the mass flux rates experienced by the HGA and the magnetometer boom will be 2.555e-2 and 8.783e-3 gram per crossing, respectively. The new flux rates are about a factor of 2 larger than those computed with M_2 = 1 gram.

multiplication factor of $\Delta = 2.52$. The corresponding ratio of the momentum of the backscattered ejecta relative to the incoming projectiles is 1.52 (to be used in Section VI).

To calculate the translational impulse imparted on the HGA, we compute the product of the mass flux rate, the impact velocity, and the momentum multiplication factor. Its magnitude is 1.329e-5 kg×31.4e+3 m/s ×2.52 ≈ 1.052 Ns. The mass of the spacecraft near the time of proximal orbit is 2,220 kg. Hence, the ΔV experienced by the spacecraft due to the momentum transferred on the HGA dish is only 0.474 mm/s. However, note that most of the dust particles will impact the HGA dish obliquely. Hence, the above estimated ΔV is an upper bound that the S/C will experience. Also, since the impulses imparted on the HGA surface is likely to be distributed uniformly and symmetrically with respect to the S/C's Z-axis, the *net* angular momenta acting about either the S/C's X or Y-axis, if any, should be negligible.

To calculate the translational impulse imparted on the magnetometer boom (that is covered with MLI), we assumed that the dust particles will perforate the MLI and landed inside magnetometer boom structure.[26] The total impulse is given by the product of the mass flux rate and the impact velocity. Its magnitude is 4.568e-6 kg×31.4e+3 m/s ≈ 0.143 Ns. The ΔV experienced by the spacecraft due to the transferred momentum on the magnetometer boom is only 0.0644 mm/s. However, the net impulse is located at a distance of 6.5 m from the S/C's Z-axis (mid point of the exposed magnetometer boom surface). Hence, the resultant angular momentum about the S/C's X-axis due to the dust collision is 0.93 Nms. During the D-ring crossing, if the S/C's attitude is controlled by the 0.52-N thrusters, the predicted firing time of each of the two attitude control thrusters (with moment arm of 1.61 m) is 0.56 s.[1] If the S/C's attitude is controlled by three reaction wheels, each with a momentum storage capacity of 34 Nms, they should be able to absorb this transient angular momentum easily.

VI. HVI on Sun sensors by Secondary Debris Produced by HVI on HGA Dish

Beside being directly impacted by dust particles travelling at high speeds, the Sun sensor covers are also threatened by some fraction of secondary debris that are produced by primary HVI of dust particles on the large parabolic HGA dish.[27,28] A schematic representation of the secondary debris for normal, oblique, and grazing HVI are depicted in Fig. 8. Sources of the secondary debris came from the disintegration of the dust particles and the HGA reflector material punched out by the direct HVI. The damage potential of a ricochet debris particle is a complex function of the spatial distributions of ricochet debris cloud, the ratio of the total ejecta mass relative to the incoming mass, as well as the velocity of the ricochet ejecta. These factors are estimated in the following paragraphs.

Fragment ejection directions can be described in terms of the cone elevation (angle between the ejecta velocity vector and the target plane, see Fig. 8) and azimuth (angle between the ejecta velocity vector projection on the target plane and a reference axis in the same plane). For normal HVI, the elevation angles measured by many authors are summarized in Ref. 23. As expected, there is a wide range of reported elevation angles: 35–70° (mean value is 52.5°). That is, the half-cone angle of the ejecta, relative to the local normal, is 37.5°. However, as noted in Ref. 23, the cone elevation angle is related to the crater depth: for a relative deeper crater (due to a higher impact velocity), the fragments are guided in a more perpendicular direction, therefore the cone elevation angle increases (and the half-cone angle decreases). The effects of projectile diameter and impact velocity on ejecta cone angle and ejecta size distribution were also investigated in Ref. 29 by striking aluminum alloy 6061-T6 targets with aluminum alloy projectile at velocities ranging from 2 to 6 km/s. Based on experimental results, the empirical relation between the half-cone angle and velocity was found to be given by ϕ_{HALF} (in deg.) ≈ $64/\sqrt{V}$ (V is in units of km/s). At V=31.4 km/s (for D-ring crossing), ϕ_{HALF} =11.42°. To be conservative, a half-cone angle of 20° is assumed in this study to account for the wide range of dispersion of the half-cone angle measured in experiments.

When Cassini assumes the HGA-to-RAM attitude, the obliquity angles of all primary HVI on the parabola dish will fall below 36.1°. Hence, it is important to study how the cone elevation angle changes with the obliquity angle. Ref. 27 provided results of a study performed to develop an empirical model that characterizes the ejecta created by an oblique HVI on a spacecraft structure. In this study, we assumed that the centerline of the ejecta cloud made an angle (relative to the target plane normal) that is identical to that of the incoming particles (the obliquity angle). With a 20-deg half-angle of the conical ejecta "cloud", the largest angle the ejecta made with the target plane normal is the sum of the obliquity angle and 20°. Based on this model, we note that only oblique HVI impacts on a small segment (called critical segment) on the large parabolic HGA dish will produce ejecta that will "land" on the small SSA cover glasses. Based on calculations reported in Appendix E, our estimate of the fraction of the primary HVI that will produce secondary ejecta that will impact the SSA cover glasses (f_{SSA}) is <0.22%.

In Ref. 23, an empirical relation for the total ejecta mass of secondary debris is given:

$$M_{ejecta}^{Total} = C \times E^{A} \cos^{2}\beta \qquad (8)$$

Here, C and A are empirical coefficients depending on both the projectile and target material, β is the obliquity angle, and E is the kinetic energy (in Joules) of the incoming projectile. Equation (8) is written in SI units. For the HGA dish materials, the coefficients C and A are estimated to be C = 2.0e-5 and A = 1 (see Table 2-1 of Ref. 23)[#]. In this study, we independently validated the usefulness of this empirical relation using data from Ref. 22. This reference provides data on secondary debris when 500-μm 4-mg steel projectiles, travelled at 1.35 km/s, impacted a 2-mm fused silica target. Based on Eq. (8), the ratio of the eject mass relative to the incoming mass, f_{Mass}, is $2.0e\text{-}5\times\frac{1}{2}\times(1.35e3)^2 \approx 18.2$. This prediction compared quite well with the ratio determined experimentally, which is 12.[22] For D-ring crossing, with β =36.1° (see Appendix E) and V =31.4 km/s, the total ejecta mass relative to the incoming mass, f_{Mass}, is 6,436. This large value came from the fact that the mass ratio is proportional to the squared velocity of the incoming projectiles (31.4 km/s in this case which is very high). This estimation is also consistent the following description of hypervelocity impact in Refs. 26–27: "*…it was demonstrated that oblique high-speed impacts generate a tremendous volume of ricochet debris,…*".

There had also been several attempts to characterize the size and velocity distributions of ricochet ejecta generated by HVI impacts. The difficulty encountered by researchers was the strong coupling between the ejecta size (mass) and ejecta velocity. That is, an observed crater can be produced by a small ejecta traveling at a high speed or by a larger ejecta traveling at a slower speed. The velocity of the ejecta could be estimated based on energy consideration. Here the assumption is that a large proportion of the projectile impact kinetic energy ends up as kinetic energy of numerous ejecta (see the conclusion section of Ref. 30).[∀] In term of the mass ratio f_{Mass}, the average ejecta velocity is $V/\sqrt{f_{Mass}} < 0.01246V$ m/s (where V is the velocity of the incoming projectile). That is, from the energy viewpoint, the ratio of ejecta velocity to incoming projectile velocity, denoted by f_{VEL}, is 1.246%. The average velocity of the ejecta could also be estimated from the momentum viewpoint. In Section V, the ratio of the momentum of the backscattered ejecta relative to the incoming projectiles is estimated to be 1.52. Hence, the average ejecta velocity is $<1.52V/f_{Mass} \approx 0.0001262V$. That is, from the momentum viewpoint, f_{VEL} = 0.01262%. To be conservative, in this study, we will use the larger value (with f_{VEL} of 1.246%). This velocity ratio estimate is in general agreement with simulation results of ejecta velocity from a 3-km/s HVI on a 2-mm spacecraft debris shield with the following velocity ratios: 2–6% for macro ejecta and 0.5–1.5% for micro ejecta.[22]

The solid angle of the ejecta cone with an apex angle $2\phi_{HALF}$ is given by $\Omega_{Ejecta} = 2\pi(1-\cos\phi_{HALF})$ steradian. Some fraction of the ejecta in this solid angle will land on the SSA cover glass. To estimate that fraction we note that each Sun sensor cover glass area is 4.6e-4/2=2.3e-4 m^2. The distance between the Sun sensor and the impact location of the direct HVI is $R_{HGA}+x_{SSA}$= 2+1.147= 3.147 m (see Fig. E2 in Appendix E). Hence the solid angle subtended by the SSA cover glass is $2.3e\text{-}4/3.147^2$ = 2.32e-5 steradian. As a fraction of the total solid angle of the ejecta, $f_{SolidAngle} = 2.32e\text{-}5/\{2\pi(1-\cos\phi_{HALF})\}$, or 3.49e-5 (where we used ϕ_{HALF} = 26.6° instead of 20° for reasons given in Appendix E).

From Sections III and IV, the integral fluence F(M) is defined as the number of dust particles with mass ≥M that impacted on spacecraft (particle counts per m^2 for one or multiple crossings). Hence, the number of dust particles with mass M per unit area is given by $-\partial F/\partial M$. If each projectile of direct HVI (with mass M) on the HGA resulted in N_{ejecta} of secondary ejecta, then the mass of each of the secondary ejecta is $M\times f_{Mass}/N_{ejecta}$. For the worst-case D-ring crossing, the total crater area due to the secondary debris, as a function of the SSA cover glass area, is estimated by Eq. (9). For N_{ejecta} =500, the attenuation factor is 7.66e-5%, and it will not impact the performance of the Sun sensors. But note that in Eq. (9), the expression we use to estimate the crater size generated by oblique impact is similar to Eq. (3) (which was an empirical expression generated using data of normal HVI). However, even if the crater diameter (due to oblique HVI) is a factor of 2 larger than that predicted by Eq. (9), the inflated attenuation factor, 7.66e-5%×2 = 15.32e-5%, will still be very small. The estimated crater depth is also given in Eq. (9). For N_{ejecta} =500, the number of dust particles that will generate secondary ejecta that can generate craters with depth >1.27 mm (half the thickness of the SSA cover glass) is 6.3e-4 particles. This is a very low probability. With larger N_{ejecta} of 1,000, 2,000, 4,000, 8,000 (and higher), the attenuation factors and damaging particle counts, given in Table 3, are equally low. In all cases, the optical attenuation factors and damaging particle counts are small. In spite of the large uncertainty of these analyses, we judge that the SSA performance is immune to secondary ejecta.

[#]These values were derived for HVI on "satellite wall" targets. For basalt target, [A,C] = [1.0,1.0e-5]. For ceramic, [A,C] = [1.0,0.9e-5], etc. See Ref. 23 for details. The [A,C] combination selected represents the worst case.

[∀]This is a very conservative assumption. In reality, a large portion of the kinetic energy is converted into energy of vaporization and ionization, resulting in small dense plasma.

A single worst-case D-ring crossing

$$F = e^{a_0} M^{a_1}, \quad a_0 = -7.7772479,\ a_1 = -0.7167029$$

$$\frac{\partial F}{\partial M} = a_1 e^{a_0} M^{a_1 - 1}$$

$$\text{Attenuation} = \frac{1}{A_{SSA}} \int_{M_C = 3.16\times10^{-7}}^{M=10^0} f_{dark} f_{SSA} f_{SolidAngle} [-\frac{\partial F_{ring}(M)}{\partial M} A_{HGA}] N_{Ejecta} \frac{\pi D^2_{SecondaryDebris}(M)}{4\times10^4} dM$$

$$= C\{M_C^{a_1+0.7066} - M^{a_1+0.7066}\} \approx 7.66\text{e-}5\% \ (\text{if } N_{ejecta} = 500) \tag{9}$$

$$\text{where } C = f_{Dark} f_{SSA} f_{SolidAngle} [\frac{A_{HGA}}{A_{SSA}}] N_{ejecta}^{0.2934} \frac{\pi \times e^{a_0}}{4\times10^4} (\frac{a_1}{a_1 + 0.7066}) \{8.037(\frac{6}{\pi\rho} f_{MASS})^{0.3533} \rho^{0.5} [f_{VEL} V\cos\theta]^{0.6667}\}^2$$

Note that:

$$P_{SecondaryDebris} = 1.0547[\frac{6M}{\pi\rho}(\frac{f_{MASS}}{N_{ejecta}})]^{0.3533} \rho^{0.5} [f_{VEL} V\cos\theta]^{0.6667} \ \text{(see also Eq. (2))}$$

$$D_{SecondaryDebris} = 8.037[\frac{6M}{\pi\rho}(\frac{f_{MASS}}{N_{ejecta}})]^{0.3533} \rho^{0.5} [f_{VEL} V\cos\theta]^{0.6667} \ \text{(See Refs. 11 and 13)}$$

M_C is the dust particle mass that will generate a crater diameter of 0.762 mm or larger.

Table 3 Damaging Particle Counts and Optical Attenuation on SSA Cover Glass due to Secondary Ejecta (Worst case D-ring Crossing with HGA-to-RAM Attitude)

Ejecta particle counts (N_{ejecta})	500	1,000	2,000	4,000	8,000	Remarks
Mass of dust particle that will create ricochet ejecta that generate HVI crater with >1.27 mm penetration depth on SSA cover glass, M_{pene}[gram]	9.25e-6	1.47e-4	2.39e-3	3.80e-2	6.13e-1	See Eq. (9)
Integral fluence of worst D-ring crossing for M_{pene} [particles per area]	1.37	0.23	3.2e-2	4.4e-3	6.0e-4	From Fig. 6
Particle counts that generate >1.27 mm penetration by secondary ejecta* [counts]	**4.38e-2**	**7.36e-3**	**1.02e-3**	**1.41e-4**	**1.92e-5**	**<<1 particle**
Mass of dust particle that will produce secondary debris that generated craters with ≥0.762 mm diameter on SSA cover glasses [gram] (M_C given in Eq. (9))	7.05e-9	1.12e-7	1.77e-6	2.87e-5	4.57e-4	-
Attenuation due to surface cratering [%]	**7.66e-5**	**7.89e-5**	**7.88e-5**	**7.25e-5**	**6.68e-5**	**Negligible****

*Total area = $A_{HGA} \times f_{SSA}$ =14.12×0.22e-2 ≈3.2e-2 m^2.
**With N_{ejecta}=16,000 and 32,000, the optical attenuations are 5.17e-5 and 2.72e-5%, respectively. The optical attenuation will fall below 272e-5% for N_{ejecta} >32,000. With N_{ejecta}= 250, the optical attenuations is 7.28e-5%. The optical attenuation will fall below 7.28e-5% for N_{ejecta} <250.

VII. Contingency Plans

As mentioned in Section III, the HGA-to-RAM spacecraft attitude will be used for five of the twenty-two proximal orbital D-ring flybys in 2017. These five orbits are orbit 1, 6–7, and 11–12 (see Table 1). During the first proximal ring plane crossing (on 4/26/17), two science instruments, RPWS and CDA, will gather data on the dust environment. These in-situ data will be used by the mission team to make quick analyses of the proximal dust environment. Results will be compared with those predicted based on remote observation data. In the event when the

estimated dust hazard is significantly worst than that was assumed in the design of the proximal orbit campaign, the spacecraft may be flown in the HGA-to-RAM attitude during all subsequent crossings (instead of just orbits 6–7 and 11–12). To this end, real-time command files must be prepared ahead of this first proximal ring plane crossing to ensure the safety of the spacecraft, at the cost of science.

During both the F/G-ring and D-ring crossings, the spacecraft's inertial attitude will be estimated using data from both the star tracker and gyroscopes. The attitude estimator will not use data from the Sun sensor. Therefore, in the unlikely event that the Sun sensor is damaged by dust HVI, transient SSA performance degradation or even complete loss of SSA data is not important to S/C attitude estimation. However, erroneous SSA data might trigger one or more SSA-based error monitors. Error monitors such are the so-called "Sun Position Discontinuity" (a sudden change in the Sun position in the S/C's body frame), "Illegitimate Sun Position Data" (loss of the Sun Presence test bit of the SSA), and/or other monitors might be triggered. The triggered error monitor will lead to unwanted Fault Protection (FP) responses.[31] One way to alleviate this risk is to send a command to mask all these Sun sensor-related monitors before the ring plane crossing. The monitors are to be unmasked, after the crossing, only after the ground team has an opportunity to confirm the performance integrity of both the prime and backup Sun sensors. The preventive remedial strategy is described in Refs. 3 and 32.

VIII. Summary and Conclusions

The "dusty" environment of several Saturn's ring regions Cassini must fly through is hazardous because of the damage dust particles, travelling at speeds as high as 31.4 km/s, can do to spacecraft hardware. During hazardous proximal ring-plane crossings, the Cassini mission operation team plans to point the high-gain antenna to the RAM vector in order to protect most of spacecraft instruments from the incoming energetic ring dust particles. However, this spacecraft attitude will expose the Sun sensors (that are mounted on the HGA dish) to the incoming dust particles. Analyses performed to quantify the risks the Sun sensors must contend with during both F/G-ring and D-ring crossings are given in this paper. Sun sensor risks studied include both the penetration damage and optical attenuation due to surface cratering caused by direct HVI of ring dust particles. Our results indicate that the probability of penetration damage of the Sun sensor cover glasses is very low even for the worst-case D-ring proximal orbit crossing. Also, the optical attenuation factor due to surface cratering of the Sun sensor cover glass caused by D-ring dust particle HVI is insignificant (0.11–0.44%). The sensor performance will not be impacted by these direct HVI of dust particles.

Beside being subjected to direct HVI of dust particles, the Sun sensor cover glasses are also threatened by secondary debris that are produced by the primary HVI of dust particles on the large HGA dish. The damage potential of ricochet debris particles is a complex function of the spatial distributions of ricochet debris cloud, the ratio of the total ejecta mass relative to the incoming mass, as well as the velocity of the secondary ejecta. With simplifying assumptions, and using results reported in Refs. 22–30, the penetration damage and optical attenuation of the Sun sensor cover glasses due to the secondary debris are also estimated in this study. Results indicated that Cassini Sun sensor performance degradation due to the secondary debris is small even for the worst-case D-ring crossing. However, the estimation uncertainty associated with the risk assessment of secondary debris is likely to be large. But we judge that the reported results are still conservative.

To better manage the SSA damage risk during selected proximal orbit crossings, it is highly desirable to follow the contingency procedures mentioned in Section VII (as well as details given in Ref. 32). These contingency procedures had been practiced for the two crossings in the SOI critical sequence as well as eleven other hazardous crossings (see Table 1, as per January 1, 2016) by the mission operation team. Based on results of risk analyses documented in this work and contingency planning work described in Ref. 32, we judge that the proximal orbit campaign will be safe from the viewpoint of dust hazard. Hence, it is highly likely that Cassini will be able to successfully complete the "*grand finale*" and bring the historic 20-year mission of Cassini to a successful end.

Acknowledgments

The work described in this paper was carried out by the Jet Propulsion Laboratory, California Institute of Technology, under contract with the National Aeronautics and Space Administration. Reference to any specific commercial product, process, or service by trade name, trademark, manufacturer, or otherwise, does not constitute or imply its endorsement by the United States Government or the Jet Propulsion Laboratory, California Institute of Technology. I want to thank my colleague, Mr. Thomas A. Burk, manager of the Cassini Attitude Control Subsystem, for his careful review of an earlier version of this paper. I also want to thank Laura L. Burke, George T.

Chen, Mickey G. Honchell, Sima Lisman, Eric J. Sturm, and Julie L. Webster, for their supports. Any remaining errors of fact or interpretation are of course the responsibility of the author.

References

[1]Lee, Allan Y. and Hanover, Gene, "Cassini Spacecraft Attitude Control System Flight Performance," Paper AIAA-2005-6269, Proceedings of the AIAA Guidance, Navigation, and Control Conference, and Exhibit, San Francisco, California, August 15–18, 2005.

[2]Buffington, B., "Proposed End-of-Mission for the Cassini Spacecraft: Inner D Ring Ballistic Saturn Impact," Paper IAC-10-C1.9.2, Proceedings of the 61st International Astronautical Congress, Prague, Czech Republic, September 27–October 1, 2010.

[3]Burk, T.A., "Cassini at Saturn Proximal Orbits – Attitude Control Challenges," Paper AIAA-2013-4710, Proceedings of the AIAA Guidance, Navigation, and Control Conference and Exhibit, August 19–22, 2013, Boston, MA.

[4]Seal, D., "Dust Hazard Management in the Outer Solar System", SpaceOps 2012; 11-15 June 2012, Stockholm, Sweden.

[5]Iyer, K.A., Mehoke, D.S., and Batra, R.C., "Interplanetary Dust Particle Shielding Capability of Spacecraft Multilayer Insulation," Journal of Spacecraft and Rockets, Vol. 50, No. 2, March-April 2015, pp. 584–594.

[6]Sevilla, D.R., "The Cassini Main Engine Assembly Cover Mechanism", Proceedings of the 31th Aerospace Mechanisms Symposium, Marshall Space Flight Center, May 1997. See also NASA NP0-20156.

[7]Sarani, S., "A Novel Methodology for Reconstruction of Titan Atmospheric Density Using Cassini Guidance, Navigation, and Control Data," Paper AIAA 2007-6343, Proceedings of the AIAA Guidance, Navigation, and Control Conference, August 20–23, Hilton Head, South Carolina, 2007.

[8]D. A., Gurnett, W. S. Kurth, D. L. Kirchner, G. B. Hospodarsky, T. F. Averkamp, P. Zarka, A. Lecacheux, R. Manning, A. Roux, P. Canu, N. Cornilleau-Wehrlin, P. Galopeau, A. Meyer, R. Bostrom, G. Gustafsson, J.-E. Wahlund, L. Aahlen, H. O. Rucker, H. P. Ladreiter, W. Macher, L. J. C. Woolliscroft, H. Alleyne, M. L. Kaiser, M. D. Desch, W. M. Farrell, C. C. Harvey, P. Louarn, P. J. Kellogg, K. Goetz, and A. Pedersen, "The Cassini Radio and Plasma Wave Science Investigation," *Space Sci. Rev.,* 114, 395–463, December 2004.

[9]Abbey, T., Carpenter, J., Read, A., and Wells, A., "Micrometeoroid Damage to CCDs in XMM-Newton and Swift and its Significance for Future X-ray Missions," Proceedings of the X-ray Universe 2005, El Escorial, Madrid, Spain, September 26–30, 2005, pp. 943–948.

[10]Cour-Palais, B.G., "Hypervelocity Impact in Metals, Glass, and Composites," International Journal of Impact Engineering, 5, pp. 221–237, 1987.

[11]Flaherty, R.E., "Impact Characteristics in Fused Silica for Various Projectile Velocities," Journal of Spacecraft and Rockets, Vol. 7, No. 3, pp. 319–324, March 1970.

[12]Hoffman, A.R., "Cassini Orbiter Functional Requirements Book: Environmental Design Requirements, Revision C," Jet Propulsion Laboratory, November 14, 1996.

[13]Christiansen, E.L., Handbook for Designing MMOD Protection, NASA/TM-2009-214785, National Technical Information Service, Springfield, VA, 2009.

[14]Chadegani, A., Iyer, K.A., Mehoke, D.S., and Batra, R.C., "Hypervelocity Impact of a Steel Microsphere on Fused Silica Sheets," International Journal of Impact Engineering, Vol. 80, June 2015, pp. 116–132.

[15]Miller, J.E., Bohl, W.E., Christiansen, E.L., Davis, B.A., and Deighton, K.D., "HVI Ballistic Limit Characterization of Fused Silica Thermal Panes," The 13th Hypervelocity Impact Symposium, 26–30 April 2015, Boulder, Colorado.

[16]Burchell, M.J. and Grey, I.D.S., "Oblique Hypervelocity Impacts on Thick Glass Targets", Material Science and Engineering A303 (2001), pp. 134–141.

[17]Edelstein, K.S., "Orbital Impact and the Space Shuttle Windshield," NASA/TM-110594, 1995.

[18]Burt, R.R. and Christiansen, E.L., "Hypervelocity Impact Testing of Transparent Spacecraft Materials," Internal Journal of Impact Engineering, Vol. 29, 2003, pp. 153–166.

[19]Paul, K.G., Igensbergs, E.B., and Berthoud, L., "Hypervelocity Impacts of Solar Cells – Observations, Experiments and Empirical Scaling Laws," International Journal of Impact Engineering," Vol. 20, 1997, pp. 627–638.

[20]Iyer, K.A., Mehoke, D.S., Chadegani, A., and Batra, R.C., "Glass Surface Spall Size Resulting From Interplanetary Dust Impacts," Proceedings of 2015 IEEE Aerospace Conference, Big Sky, Montana, March 7–14, 2015.

[21]Taylor, E.A. and McDonnell, J.A.M., "Hypervelocity Impact on Soda Lime Glass: Damage Equations for

Impactors In the 400–2000 Micron Range," Advanced Space Research, Vol. 20, No. 8, pp. 1457–1460, 1997.

[22]Michel, Y., Chevalier, J.M., Durin, C., Espinosa, C., and Malaise, F., "Hypervelocity Impacts on Thin Brittle Targets: Experimental Data and SPH Simulation," Hypervelocity Impact Symposium, 10–14 October 2005, Lake Tahoe, California.

[23]Christiansen, E., Flegel, S., Francesconi, A., Higaside, M., Krisko, P., Mandeville, J.C., and Meshcheryakov, S., "Characterization of Ejecta From HVI On Spacecraft Outer Surfaces," Inter-agency Space Debris Coordination Committee, IADC-11-05, April 2013.

[24]Hoerth, T., Schäfer, F., Hupfer, J., Millon O., and Wickert, M., "Momentum Transfer in Hypervelocity Impact Experiments on Rock Targets," 13th Hypervelocity Impact Symposium, Procedia Engineering, 103 (2015), pp. 197–204, 2013.

[25]Dauksys, R.J., Pagano, N.N., and Spain, R.G., "Graphite Fiber/Epoxy Resin Matric Composites," technical Report AFML-TR-67-367, Air Force Materials Laboratory, Wright-Patterson Air Force Base, Ohio, April 1968.

[26]Triolo, J.J. and Ousley, G.W., "Returned Solar Max Hardware Degradation Study Results," NASA/SDIO Space Environmental Effects on Materials Workshop, NASA Langley Research Center; May 1989; pp. 133-159.

[27]Schonberg, W.P., "Characterizing Secondary Debris Impact Ejecta," International Journal of Impact Engineering, 26 (2001), pp. 713–724.

[28]Schonberg W.P. and Taylor R.A., "Exterior Spacecraft Subsystem Protective Shielding Analysis and Design," Journal of Spacecraft and Rockets, Vol. 27, No. 3, May-June, 1990, pp. 267–274.

[29]Nishida, M., Hiraiwa, Y., Hayashi, K., and Hasegawa, S., "Ejecta Cone Angle and Ejecta Size Following a Non-perforating Hypervelocity Impact," 2015 Hypervelocity Impact Symposium, Procedia Engineering, 103, pp. 444–449, 2015.

[30]Woodward, R.L., Gooch, W.A., Jr., O'Donnell, R.G., Perciballi, W.J., Baxter, B.J., and Pattie, S.D., "A Study of Fragmentation in the Ballistic Impacts of Ceramics," International Journal of Impact Engineering, Vol.15, No. 5, pp. 605-618, 1994.

[31]Brown, G. Mark and Johnson, S. A., "An Overview of the Fault Protection Design for the Attitude Control Subsystem of the Cassini Spacecraft," Proceedings of the 1998 American Control Conference, Philadelphia, Pennsylvania, June 24–26,1998.

[32]Bates, D., "Cassini Operational Sun Sensor Risk Management During Proximal Orbit Saturn Ring Plane Crossings," Proceedings of the 2016 AIAA Science and Technology Forum and Exposition, 4–8 January 2016, San Diego, California.

[33]Srama , R., Kempf, S., Moragas-Klostermeyer, G., Altobelli, N., Auer, S., Beckmann, U., Bugiel, S., Burton, M., Economomou T., et al, "The Cosmic Dust Analyzer Onboard Cassini: Ten Years of Discoveries," CEAS Space Journal (2011) 2:3–16.

Appendix A
HVI Penetration Results at High Impact Velocity (Ref. 15)

Ref. 15 documented results from hypervelocity impact testing using the NASA JSC Hypervelocity Impact Technology Laboratory (HITL) and the Lockheed Martin Space Systems Company, up to 10 km/s on a fused silica window system proposed for the Orion spacecraft. Test results were augmented by simulation results performed with the Sandia National Laboratories three dimensional hydrodynamics simulation tool CTH Version 9.1. Fig. A1 (from Fig. 4 of Ref. 15) depicts the variations of the critical diameters with the impact velocity (to as high as 30 km/s). The critical diameter of the projectile is defined as the projectile diameter that will generate a penetration depth of 1.27 cm.[15]

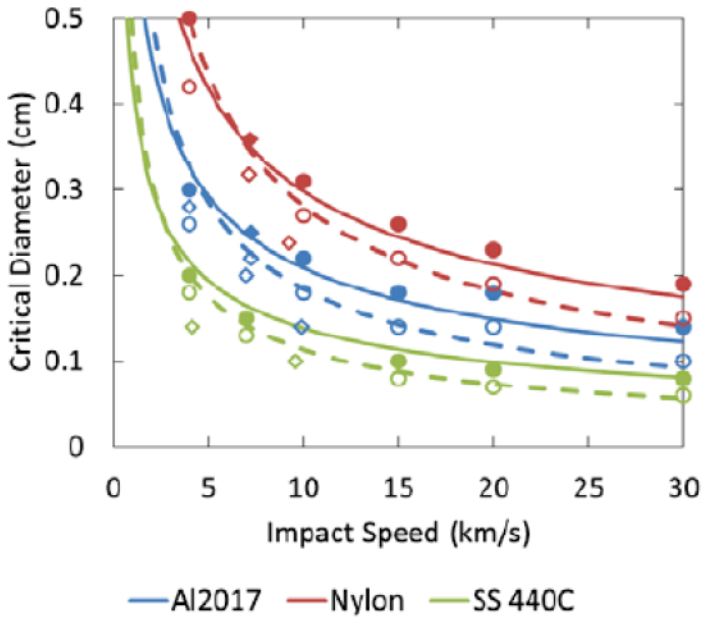

Fig. A1. Variations of the critical diameters with the impact velocity (see Fig. 4 of Ref. 15). (Solid line is based on data from Ref. 15, with test data drawn as diamonds and simulation data drawn as circles. The dashed lines show the heritage ballistic limit equation results from Refs. 11 and 13). Projectile materials used are steel (green), aluminum (red), and nylon (blue).

In Fig. A1, the solid line is based on data from Ref. 15, with test data drawn as diamonds and simulation data drawn as circles. The dashed lines show the heritage ballistic limit equation results from Refs. 11 and 13. For impact velocity > 5 km/s, we note that the dashed line is below its solid-line counterpart. For example, at impact velocity of 30 km/s, the ratio R of the critical diameter (predicted by heritage formula) to the critical diameter (via test or hydrodynamic simulations) is 0.75 (for steel spherical projectiles). The ratios are 0.79 and 0.80 for aluminum and nylon spherical projectiles, respectively. That is, on the average, the critical projectile diameter computed using the heritage formula is 78% of that determined via test (or hydrodynamic simulation).

For the same penetration depth (1.27 cm, as stated above) and at the same impact velocity, the heritage equation[11,13] predicted that the required projectile diameter is smaller than that found experimentally (or via hydrodynamic simulation). That is, the penetration depth predicted by Eq. (2) (in Section III) is <u>conservative</u> (over-predicted by a factor of $1/0.78^{1.06} \approx 1.30$) even for impact velocity as high as 30 km/s. Selected test results from Ref. 15 are tabulated in Table A1 to illustrate this observation. Looking at the first row of Table A1, the penetration depth on a glass pane due to1.4-mm aluminum (Al 2740-T4, with density of 2.79 gram/cc) projectile travelling at a speed of 9.89 km/s was found to be 5 mm experimentally. But according to Eq. (2), the penetration depth is predicted to be 10.2 mm. That is, Eq. (2) over-predicted the penetration depth by a factor of about 2.03. Different over-prediction factors are found for other tests (see the other five test cases tabulated in Table A1) but in all cases, the over-prediction factor is >1.

Table A1
A Comparison of Predicted Penetration Depth with Experimental Results
(Raw data came from Ref. 15)

Test reported in Ref. 15	Projectile Density [gram/cc]	Impact Velocity [km/s]	Projectile diameter [cm]	Penetration depth [Experimental results, cm]	Penetration Depth [predicted by Ref. 11, cm]	Over-prediction factor [-]
HITF13244	2.796	9.89	0.14	0.5	1.02	2.03
HITF13243	1.146	9.23	0.238	0.73	1.09	1.50
HITF13245	7.650	9.56	0.10	0.74	1.15	1.55
HITF14084	2.796	7.22	0.22	1	1.33	1.33
HITF14081	7.650	4.11	0.14	0.43	0.94	2.18
HITF14076	2.796	3.97	0.28	0.86	1.15	1.34

*Assumed densities of aluminum (Al 2017-T4), nylon, and steel (SS 440C) projectiles are 2.796, 1.146, and 7.65 gram/cm^3, respectively.

Based on these results, we concluded that even though the regression relation Eq. (2) was generated based on HVI tests performed with $6.0 \le V \le 7.5$ km/s, its prediction is equally applicable for both the SOI ring-plane crossing scenario (with dust impact speed as high as 17.1 km/s) and the proximal orbit scenario (with dust impact speed as high as 31.4 km/s), with different degrees of conservativeness.

Appendix B
SSA Optical Attenuation Error due to HVI Craters Generated By F/G-ring Crossings
(Using Formulae from Ref. 11)

An approximate upper bound of the integral fluence (for all ring plane crossings of the Cassini prime mission) depicted in Fig. 6 could be determined, and the partial $\partial F/\partial M$ could be computed accordingly. For $\rho = 0.5$ gram/cc and $V = 13.6$ km/s, the optical attenuation error is about 0.037%. If the density is quadrupled, the optical attenuation error is slightly larger, at 0.064%.

$$\log_e F = a_0 + a_1 \log_e M, \quad F = e^{a_0} M^{a_1}, \qquad a_0 = -10.961,\ a_1 = -0.973$$

$$\frac{\partial F}{\partial M} = a_1 e^{a_0} M^{a_1 - 1}$$

$$D_e = 8.037\left[\frac{6M}{\pi\rho}\right]^{0.3533} \rho^{0.5} V^{0.6667} \text{ (See Ref. 11)}$$

$$\text{Attenuation} = \frac{2}{A_{SSA}} \int_{M_1 = 0.955\times10^{-8}}^{M_2 = 1} f_{Dark}\left[-\frac{\partial F}{\partial M} A_{SSA}\right]\left[\frac{\pi D_e^2(M)}{4\times10^4}\right] dM \qquad \text{(B1)}$$

$$= C\{M_2^{a_1+0.7066} - M_1^{a_1+0.7066}\} \approx 0.037\%$$

$$\text{where } C = 2 f_{Dark} \frac{\pi \times e^{a_0}}{4\times10^4}\left[-\left(\frac{a_1}{a_1 + 0.7066}\right)\left\{8.037\left(\frac{6}{\pi\rho}\right)^{0.3533} \rho^{0.5} V^{0.6667}\right\}^2\right]$$

$\rho = 0.5$ gram/cc, and $f_{Dark} = 0.1$, $V = 13.6$ km/s.

For $\rho = 2.0$ gram/cc, and $V = 13.6$ km/s., M_1 is 0.535e-8 gram.

The corresponding optical attenuation is 0.064%

Appendix C
SSA Optical Attenuation Error due to HVI Craters From F/G-ring Crossings
(Using Formulae from Ref. 18)

For ρ = 0.5 gram/cc and V = 13.6 km/s, the crater diameter could be estimated using relation given in Ref. 18 (see also Eq. (5)). The corresponding optical attenuation error is about 0.089%. If the density is quadrupled, the optical attenuation error is 0.083%. Note in Eq. (C1), the two terms in the parameter C that are related to the density, $\rho^{-0.394}$ and $\rho^{0.375}$ almost cancel each other. Hence, the optical attenuation factor isn't a strong function of the dust particle density.

$$\log_e F = a_0 + a_1 \log_e M, \quad F = e^{a_0} M^{a_1}, \qquad a_0 = -10.961,\ a_1 = -0.973$$

$$\frac{\partial F}{\partial M} = a_1 e^{a_0} M^{a_1 - 1}$$

$$D_e = 9.656\left[\frac{6M}{\pi\rho}\right]^{0.394} \rho^{0.375} V^{0.915} \text{ (Ref. 18)}$$

$$\text{Attenuation} = \frac{2}{A_{SSA}} \int_{M_1=0.549\times10^{-8}}^{M_2=1} f_{Dark}\left[-\frac{\partial F}{\partial M} A_{SSA}\right]\left[\frac{\pi D_e^2(M)}{4\times10^4}\right] dM \qquad \text{(C1)}$$

$$= C\{M_2^{a_1+0.788} - M_1^{a_1+0.788}\} \approx 0.089\%$$

$$\text{where } C = 2 f_{Dark} \frac{\pi \times e^{a_0}}{4\times10^4}\left[-\left(\frac{a_1}{a_1+0.788}\right)\left\{9.656\left(\frac{6}{\pi\rho}\right)^{0.394} \rho^{0.375} V^{0.915}\right\}^2\right]$$

$\rho = 0.5$ gram/cc, f_{Dark}=0.1, and V = 13.6 km/s.

For $\rho = 2.0$ gram/cc, and V = 13.6 km/s., M_1 is 0.591e-8 gram.

The corresponding optical attenuation is 0.083%

Appendix D
SSA Optical Attenuation Error due to HVI Craters From D-ring Crossings
(Using Formulae from Refs. 11 and 18)

An approximate relation for the integral fluence of all D-ring crossings is given in Section IV. From it, one can derive the partial $\partial F/\partial M$. For ρ = 1.0 gram/cc and V = 31.4 km/s, the optical attenuation error is about 0.998% (see Eq. (D1).

$$
\begin{aligned}
&F = e^{a_0}M^{a_1}, \qquad a_0 = -5.5289069,\ a_1 = -0.7148596 \\
&\text{(All D-ring crossings)} \\
&\frac{\partial F}{\partial M} = a_1 e^{a_0} M^{a_1 - 1} \\
&\rho = 1.0 \text{ gram/cc},\ f_{Dark} = 0.1, \text{ and } V = 31.4 \text{ km/s}. \\
&D_e = 8.037\left[\frac{6M}{\pi\rho}\right]^{0.3533} \rho^{0.5} V^{0.6667} \text{ (Ref. 11)} \\
&\text{Attenuation} = \frac{2}{A_{SSA}} \int_{M_1 = 1.49\times10^{-9}}^{M_2 = 1} f_{Dark}\left[-\frac{\partial F}{\partial M} A_{SSA}\right]\left[\frac{\pi D_e^2(M)}{4\times10^4}\right] dM \\
&= C\{M_2^{a_1+0.7066} - M_1^{a_1+0.7066}\} \approx 0.998\% \\
&\text{where } C = 2 f_{Dark} \frac{\pi \times e^{a_0}}{4\times10^4}\left[-\left(\frac{a_1}{a_1+0.7066}\right)\left\{8.037\left(\frac{6}{\pi\rho}\right)^{0.3533} \rho^{0.5} V^{0.6667}\right\}^2\right]
\end{aligned}
\tag{D1}
$$

Similarly, for the integral fluence of the worst-case D-ring crossing, the optical attenuation error is about 0.1076% (see Eq. (D2).

$$
\begin{aligned}
&F = e^{a_0}M^{a_1}, \qquad a_0 = -7.7772479,\ a_1 = -0.7167029 \\
&\frac{\partial F}{\partial M} = a_1 e^{a_0} M^{a_1 - 1} \\
&\rho = 1.0 \text{ gram/cc},\ f_{Dark} = 0.1, \text{ and } V = 31.4 \text{ km/s}. \\
&D_e = 8.037\left[\frac{6M}{\pi\rho}\right]^{0.3533} \rho^{0.5} V^{0.6667} \text{ (see Ref. 11)} \\
&\text{Attenuation} = \frac{2}{A_{SSA}} \int_{M_1 = 1.49\times10^{-9}}^{M_2 = 1} f_{Dark}\left[-\frac{\partial F}{\partial M} A_{SSA}\right]\left[\frac{\pi D_e^2(M)}{4\times10^4}\right] dM \\
&= C\{M_2^{a_1+0.7066} - M_1^{a_1+0.7066}\} \approx 0.1076\% \\
&\text{where } C = 2 f_{Dark} \frac{\pi \times e^{a_0}}{4\times10^4}\left[-\left(\frac{a_1}{a_1+0.7066}\right)\left\{8.037\left(\frac{6}{\pi\rho}\right)^{0.3533} \rho^{0.5} V^{0.6667}\right\}^2\right]
\end{aligned}
\tag{D2}
$$

Using the worst-case HVI models from Ref. 18, and for the worst-case D-ring crossing, the optical attenuation error is about 0.4371% (see Eq. (D3)).

$$F = e^{a_0} M^{a_1}, \qquad a_0 = -7.7772479,\ a_1 = -0.7167029$$

A single worst-case D-ring crossing

$$\frac{\partial F}{\partial M} = a_1 e^{a_0} M^{a_1 - 1}$$

$\rho = 1.0$ gram/cc, $f_{Dark} = 0.1$, and V = 31.4 km/s.

$$D_e = 9.656[\frac{6M}{\pi\rho}]^{0.394} \rho^{0.375} V^{0.915} \text{ (see Ref. 18)} \tag{D3}$$

$$\text{Attenuation} = \frac{2}{A_{SSA}} \int_{M_1 = 8.1\times10^{-10}}^{M_2 = 1} f_{Dark}[-\frac{dF}{dM} A_{SSA}][\frac{\pi D_e^2(M)}{4\times10^4}]\, dM$$

$$= C\{M_2^{a_1+0.788} - M_1^{a_1+0.788}\} \approx 0.4371\%$$

where $C = 2f_{Dark} \frac{\pi \times e^{a_0}}{4\times10^4}[-(\frac{a_1}{a_1 + 0.788})\{9.656(\frac{6}{\pi\rho})^{0.394} \rho^{0.375} V^{0.915}\}^2]$

$\rho = 1$ gram/cc, $f_{Dark} = 0.1$, and V = 31.4 km/s.

Note that M1 is 8.1e-10 gram because it will generate a crater diameter of 0.762 mm

Appendix E
Secondary Debris from HVI of Dust Particles on High Gain Antenna

The radius of the Cassini HGA dish (R_{HGA}) is about 2 m at the rim, and the depth (D_{HGA}) is about 0.73 m. Hence, with reference to Fig. E1, the HGA surface z(x), and the corresponding obliquity angle (β) are given by the following expressions:

$$z(x) = \frac{D_{HGA}}{R_{HGA}^2} x^2 \qquad \text{(E1)}$$

$$\frac{dz}{dx}(x) = \frac{2D_{HGA}}{R_{HGA}^2} x$$

$$\beta\,(x) = \tan^{-1}\{\frac{2D_{HGA}}{R_{HGA}^2} x\}$$

At the rim of the HGA dish (where x = ±2 m), the obliquity angle is $\tan^{-1}\{2\times0.73\times2/2^2\} = 36.13^\circ$. Only oblique HVI impacts on a small segment (called critical segment) of the parabolic HGA dish will produce ricochet ejecta that will "land" on the small SSA cover glasses, obliquely. An estimate of the size of this critical segment, as a fraction of the total surface area of the HGA dish (14.12 m^2), is given in this appendix.

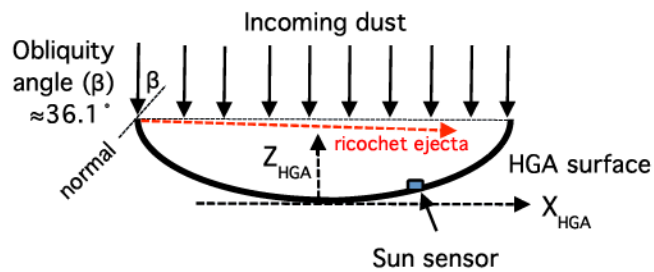

Fig. E1. Ricochet ejecta from HVI of dust particles on high gain antenna dish (Not to scale. An illustration only)

In Fig. E2, α_E denotes the ejecta angle (relative to the HGA Z-axis), and α_{SSA} denotes the angle from the HVI impact point to the SSA cover location (where x_{SSA}=1.147 m and z_{SSA}= 0.24 m).

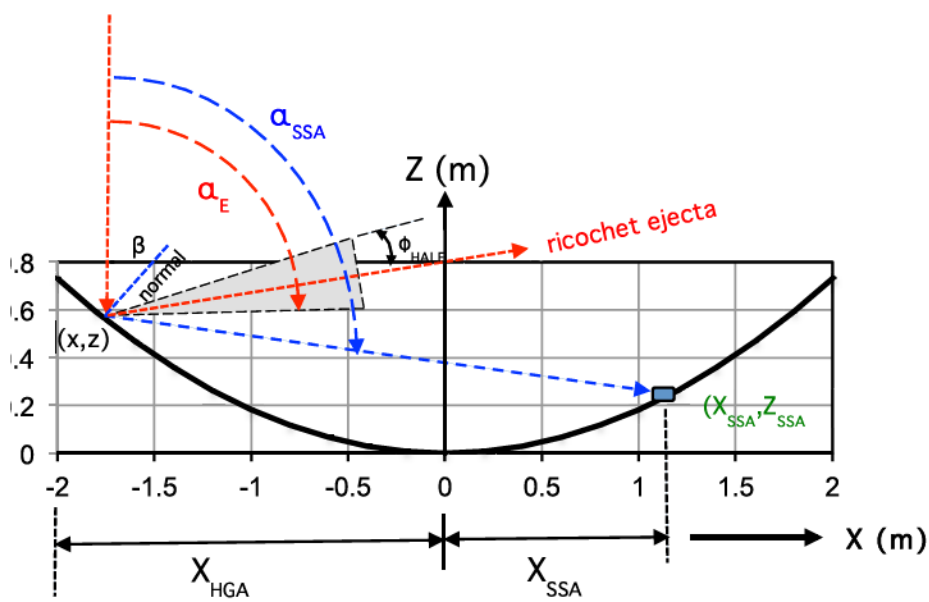

Fig. E2. Definitions of the α_E and α_{SSA} Angles (see also Eq. (E2))

For $-R_{HGA} \leq x \leq 0$, the two angles are given by:

$$\alpha_{SSA}(x,z) = \tan^{-1}\{\frac{z-z_{SSA}}{x_{SSA}-x}\} + \frac{\pi}{2}$$

$$\beta(x) = \tan^{-1}\{\frac{2D_{HGA}}{R_{HGA}^2}x\} \qquad \text{(E2)}$$

$$\alpha_E(x,z) = 2\beta(x) + \phi_{HALF}$$

The expression for the ejecta angle (α_E) is derived based on the assumption that the centerline of the ejecta cloud made an angle (relative to the target plane normal) that is identical to that of the incoming particles (the obliquity angle). With a 20-deg half-angle of the conical ejecta "cloud", the largest angle the ejecta made with the target plane normal is the sum of the obliquity angle and 20° (see Section V). With these assumptions, the variations of the angles α_E and α_{SSA}, as function of the HGA x-axis coordinate, are given in Fig. E3. Clearly, α_{SSA} is larger than α_E for all ricochet ejecta generated by primary HVI on the entire HGA surface. No ricochet ejecta from impact on HGA surface with $-R_{HGA} \leq x \leq 0$ (as well as $0 \leq x \leq +R_{HGA}$) will impact the SSA cover glasses. Only when ϕ_{HALF} is larger than 26.6° will there be some impact. The corresponding obliquity angle on the SSA cover glass is $\tan^{-1}\{(R_{HGA}+x_{SSA})/(D_{HGA}-z_{SSA})\} \approx 81.15°$.

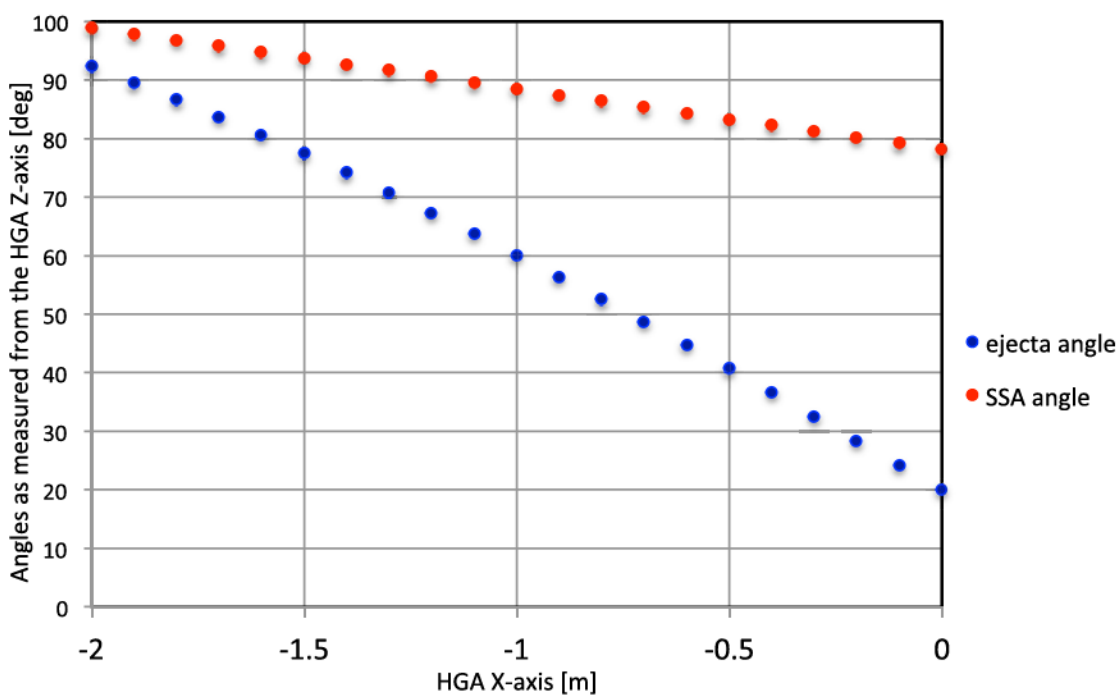

Fig. E3. Variations of the Ejecta and SSA Angles with HGA Horizontal Axis (with an assumed ejecta cloud half cone angle of 20°)

To be conservative, let us increase ϕ_{HALF} from 20° to 26.6°. With this larger ϕ_{HALF}, ricochet ejecta from HVI on a small HGA segment $-2 \leq x \leq -1.99$ m will produce ejecta that will land on the SSA cover glass. The radial "dimension" of this critical surface is 0.01 m. The width of this swath is at most $\pm(R_{HGA}+x_{SSA})\times\tan(\phi_{HALF}) \approx \pm 1.5758$ m. The approximate area of the critical segment is 0.0315 m^2, which is about 0.22% of the total surface area of the parabolic dish. Based on these conservative calculations, our estimate of the fraction of the primary HVI that will ricochet ejecta landing on the SSA cover glasses (f_{SSA}) is <0.22%.